required in calculating multi-dimensional integrals. This will make the calculation very efficient. The neural network is inherently a black box of nonlinear mapping and thus it can model strongly nonlinear functions. Since the integrand is replaced by the neural network output during integration, one needs not to know about the overall characteristic of the integrand. Although the training work of a neural network in modeling the integrand function may be time consuming, it can be finished in advance. The trained neural network for integrands will make the computation of multi-dimensional integrals almost real-time. Furthermore, the proposed method is independent of the integrand function. Therefore, the proposed method is very useful and can be extended to calculate many other engineering problems with complicated and multi-dimensional integrals.

ACKNOWLEDGMENT

The author would like to express his sincere gratitude to the National Center for High-Performance Computing, and the China Motor Corporation, both in Taiwan, for supporting the research resource.

KUN-CHOU LEE
Dept. of Systems and Naval Mechatronic Engineering
National Cheng-Kung University
Tainan, 701
Taiwan
E-mail: (kclee@mail.ncku.edu.tw)

REFERENCES

[1] Lee, J., Seo, I., and Han, S. M.
Radiation power estimation for sonar transducer arrays considering acoustic interaction.
Sensors and Actuators A: Physical, **90**, 1–2 (May 2001), 1–6.

[2] Swenson, G. W., and Johnson, W. E.
Radiation impedance of a rigid square piston in an infinite baffle.
The Journal of the Acoustical Society of America, **24** (1952), 84.

[3] Arase, E. M.
Mutual radiation impedance of square and rectangular pistons in a rigid infinite baffle.
The Journal of the Acoustical Society of America, **36**, 8 (Aug. 1964), 1521–1525.

[4] Lee, J., and Seo, I.
Radiation impedance computations of a square piston in a rigid infinite baffle.
Journal of Sound and Vibrations, **198**, 3 (1996), 299–312.

[5] Li, W. L., and Gibeling, H. J.
Determination of the mutual radiation resistances of a rectangular plate and their impact on the radiation sound power.
Journal of Sound and Vibrations, **229**, 5 (2000), 1213–1233.

[6] Li, W. L.
An analytical solution for the self- and mutual radiation resistances of a rectangular plate.
Journal of Sound and Vibrations, **245**, 1 (2001), 1–16.

[7] Haykin, S.
Neural networks—Comprehensive Foundation.
Englewood Cliffs, NJ: Prentice-Hall, 1999.

[8] Christodoulous, C., and Georgiopoulos, M.
Applications of Neural Networks in Electromagnetics.
Boston: Artech House, 2001.

[9] Zhang, Q. J., and Gupta, K. C.
Neural Networks for RF and Microwave Design.
Boston: Artech House, 2000.

[10] Lee, K. C.
Mutual coupling analyses of antenna arrays by neural network models with radial basis functions.
Journal of Electromagnetic Waves and Applications, **17**, 8 (Aug. 2003), 1217–1223.

[11] Lee, K. C.
A neural network based model for the two dimensional microwave imaging of cylinders.
International Journal of RF and Microwave Computer-Aided Engineering, **14**, 5 (Sept. 2004), 398–403.

[12] Lee, K. C., and Lin, T. N.
Application of neural networks to analyses of nonlinearly loaded antenna arrays including mutual coupling effects.
IEEE Transactions on Antennas Propagation, **53**, 3 (Mar. 2005), 1126–1132.

[13] Specht, D. F.
A general regression neural network.
IEEE Transactions on Neural Networks, **2** (Aug. 1996), 568–576.

Improved Global Range Alignment for ISAR

An improved global range alignment is presented for inverse synthetic aperture radar (ISAR) imaging. The shifts of the echoes are modeled as a polynomial, and the coefficients of this polynomial are chosen to optimize a quality measure of range alignment. The shift in the time domain is carried out by introducing a phase ramp in the frequency domain in order to remove the limitation of integer steps. Because the quality measure of range alignment is calculated directly in the frequency domain, this method is computationally more efficient than the original global method.

I. INTRODUCTION

Inverse synthetic aperture radar (ISAR) uses the motion between the radar and the target to image the target. The radar can be ground based, airborne, or space borne. The platform can be stationary or

Manuscript received April 21, 2005; revised May 11, 2006; released for publication January 7, 2007.

IEEE Log No. T-AES/43/3/908411.

Refereeing of this contribution was handled by V. C. Chen.

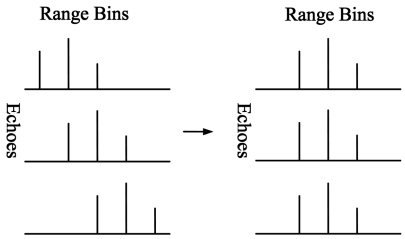

Fig. 1. Range alignment.

moving. The beam tracks moving targets of interest. The targets range from man-made objects like ships, airplanes, and satellites to natural objects like moons and planets.

There are various algorithms for ISAR imaging [1]. Here we only discuss the range-Doppler algorithm, which applies to a small rotational angle. For a large rotational angle, typical algorithms include the subaperture algorithm, the subpatch algorithm, the polar-format algorithm and the back-projection algorithm.

The range-Doppler algorithm has three steps. First, the scatterers with different ranges are resolved using their differences in time delay. Usually, a wide-band technique like the matched-filter technique, the stretch technique or the stepped-frequency technique is used to improve range resolution [2–3]. Then, translation compensation is used to remove the effect of the translation between the radar and the target in range. Finally, in each range bin, the scatterers with different azimuths are resolved using their differences in Doppler frequency. The most widely used method is the Fourier transform. Other methods include modern spectral estimation [4] and time-frequency representation [5].

Translation compensation is a key step in ISAR imaging. It consists of range alignment and phase adjustment. In range alignment, the signals from the same scatterer are aligned in range by shifting the echoes. If no prior knowledge is available about the translation, range alignment can be achieved using the similarity of the envelopes of the echoes. (See Fig. 1. For clarity, only the amplitude of the signal is shown.) Typical methods include the peak method [6], the maximum-correlation method [6], the frequency-domain method [6], the Hough-transform method [7], the minimum-entropy method [8] and the global method [9]. Phase adjustment is used to remove the translational Doppler phase. Typical methods for phase adjustment include the dominant-scatterer method [6], the scattering-centroid method [3], the phase-gradient method [10, 11], the time-frequency method [12], the maximum-contrast method [13] and the minimum-entropy method [8, 14, 15]. These methods apply even if no prior knowledge is available about the translation. Additionally, range alignment and phase adjustment can also be implemented together in the domain of slow time and the frequency with respect to fast time. The minimum-entropy translation compensation, which applies even with no prior knowledge about the translation, is based on this scheme [2].

As shown in [9], the global method is superior to the commonly used methods like the peak method and the maximum-correlation method in the quality of range alignment. In the global method, the quality of range alignment is measured by the energy of the sum envelope. The better the quality of range alignment is, the larger the energy of the sum envelope. The shifts of the echoes are modeled as a polynomial, and the coefficients of this polynomial are chosen to maximize the energy of the sum envelope. The shift in the time domain is achieved by introducing a phase ramp in the frequency domain in order to remove the limitation of integer steps. In the original version, the spectra of the echoes or the spectra of the envelopes need to be transformed into the time domain to calculate the energy of the sum envelope. It is time consuming. We present a frequency-domain expression here for the energy of the sum envelope so that it can be calculated directly from the spectra of the envelopes. This significantly raises the computational efficiency of the algorithm. In some applications, like real-time tracking, imaging and classification of moving targets, a high computational efficiency is very important. A brief description of this work has been given in [16].

II. IMPROVED GLOBAL RANGE ALIGNMENT

A. Quality Measure of Range Alignment

The quality of range alignment can be measured by the energy of the sum envelope. The sum envelope is defined as

$$s(t) = \sum_{m=0}^{M-1} a_m(t - t_m) \tag{1}$$

where t is fast time, m and M are the index and the number of the echoes, respectively, $a_m(t)$ is the envelope of echo m, i.e., the amplitude of echo m, and t_m is the shift made to echo m. The energy of $s(t)$ is defined as

$$E = \int_{-\infty}^{\infty} s(t)^2 dt. \tag{2}$$

It can be shown that when all the echoes are aligned, E is maximum [9]. Substituting (1) into (2), we obtain

$$E = E_0 + 2\sum_{m=0}^{M-2}\sum_{l=m+1}^{M-1} c(m,l) \tag{3}$$

where E_0 is the total energy of the envelopes of the echoes, i.e.,

$$E_0 = \sum_{m=0}^{M-1} \int_{-\infty}^{\infty} a_m(t)^2 dt \tag{4}$$

and $c(m,l)$ is the correlation of the envelopes of echoes m and l, i.e.,

$$c(m,l) = \int_{-\infty}^{\infty} a_m(t - t_m) a_l(t - t_l) dt. \tag{5}$$

E_0 is a constant. Different echoes have similar envelopes. When all the echoes are aligned, every $c(m,l)$ is maximum and thus E is maximum.

Applying Parseval's equation to (2), we obtain

$$E = \frac{1}{2\pi} \int_{-\infty}^{\infty} |S(\omega)|^2 d\omega \tag{6}$$

where $S(\omega)$ is the spectrum of $s(t)$. Taking the Fourier transform of (1), we obtain

$$S(\omega) = \sum_{m=0}^{M-1} A_m(\omega) \exp(-j\omega t_m) \tag{7}$$

where $A_m(\omega)$ is the spectrum of $a_m(t)$.

The integral in (6) is approximated as a sum based on the definition of an integral, i.e.,

$$E = \frac{1}{NT} \sum_{k=-\infty}^{\infty} \left| S\left(\frac{2\pi}{NT} k\right) \right|^2 \tag{8}$$

where N is the number of the range bins, k is the index of ω, and T is the sampling period of t. Since $s(t)$ is real, $S(\omega)$ is conjugate symmetric about $\omega = 0$. Thus, (8) is also expressed as

$$E = \frac{1}{NT} \left[|S(0)|^2 + 2 \sum_{k=1}^{\infty} \left| S\left(\frac{2\pi}{NT} k\right) \right|^2 \right]. \tag{9}$$

As the quality measure of range alignment, (9) has the simplified form

$$E' = \sum_{k=1}^{\infty} \left| S\left(\frac{2\pi}{NT} k\right) \right|^2. \tag{10}$$

Assume that $S(\omega) = 0$ if $|\omega| \geq \pi/T$. Then, (10) is written as

$$E' = \sum_{k=1}^{N/2-1} \left| S\left(\frac{2\pi}{NT} k\right) \right|^2. \tag{11}$$

The quality of range alignment is measured by (11) in the improved global method. The discrete form of (7) is used to calculate $S(\cdot)$ in (11), i.e.,

$$S\left(\frac{2\pi}{NT} k\right) = \sum_{m=0}^{M-1} A_m\left(\frac{2\pi}{NT} k\right) \exp\left(-j \frac{2\pi}{N} k n_m\right), \quad 1 \leq k \leq \frac{N}{2} - 1 \tag{12}$$

where n_m is the normalized shift made to echo m, i.e., $n_m = t_m/T$. $A_m(\cdot)$ in (12) is calculated using the fast Fourier transform for a real sequence.

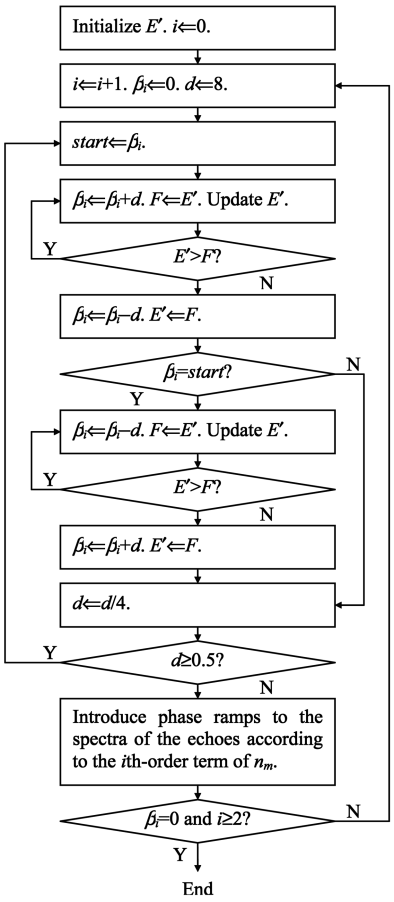

Fig. 2. Estimation of β_i.

B. Algorithm

n_m is modeled as a polynomial, i.e.,

$$n_m = \sum_{i=1}^{\infty} \beta_i \left(\frac{2m}{M} - 1\right)^i, \qquad 0 \leq m \leq M - 1 \tag{13}$$

where β_i is the coefficient to be estimated. Here, the zero-order term is ignored because it is trivial to range alignment.

β_i is estimated by the algorithm in Fig. 2. First, β_1 is increased step by step until E' is maximized. If it cannot be increased by even one step, β_1 is decreased step by step until E' is maximized. Then, the above process is repeated for smaller step sizes. Next, β_2, β_3 and so on are adjusted in the same way. The order of n_m is adaptive, and is assumed to be high enough when $\beta_i = 0$ and $i \geq 2$.

The minimum step size of β_i should be chosen to achieve a good tradeoff between the estimation accuracy and the computational efficiency. The smaller the minimum step size is, the higher the estimation accuracy. However, because more steps may be needed, the computational efficiency may be lower. In our processing, the minimum step size of β_i is chosen as 0.5. The initial step size and the decrease factor of β_i should be chosen to have a small number

of steps and thus a high computational efficiency. Actually, there exists a large freedom in choosing the two parameters. In our processing, the initial step size of β_i is chosen as 8, and the decrease factor of β_i is chosen as 4.

Since it aligns all the echoes globally, this algorithm is robust against noise and target scintillation and avoids error accumulation. In addition, in this algorithm, the shift in the time domain is implemented by introducing a phase ramp in the frequency domain, which removes the limitation of integer steps.

C. Comparison with Original Global Range Alignment

The integral in (2) is approximated as a sum based on the definition of an integral, i.e.,

$$E = T \sum_{n=-\infty}^{\infty} s(nT)^2. \tag{14}$$

As the quality measure of range alignment, (14) has the simplified form

$$E'' = \sum_{n=-\infty}^{\infty} s(nT)^2. \tag{15}$$

Assume that $s(t) = 0$ if $t < 0$ or $t \geq NT$. Then, (15) is written as

$$E'' = \sum_{n=0}^{N-1} s(nT)^2. \tag{16}$$

Equation (16) is used to measure the quality of range alignment in the original global method [9]. The discrete form of (1) is used to calculate $s(\cdot)$ in (16), i.e.,

$$s(nT) = \sum_{m=0}^{M-1} a_m[(n - n_m)T], \qquad 0 \leq n \leq N-1. \tag{17}$$

In both the original and the improved global methods, the shift in the time domain is implemented by introducing a phase ramp in the frequency domain in order to remove the limitation of integer steps. The original global method uses (16) to measure the quality of range alignment, and the spectra of the echoes or the spectra of the envelopes have to be transformed into the time domain to calculate (16). It is time consuming. However, in the improved global method, (11) is used to measure the quality of range alignment and can be calculated directly from the spectra of the envelopes. This improves the computational efficiency of the algorithm significantly.

III. RESULTS

As shown in [9], the global method results in better quality of range alignment than the commonly used methods like the peak method and the maximum-correlation method. We show in this section that the improved global method is similar to the global method in the quality of range alignment but has a higher computational efficiency.

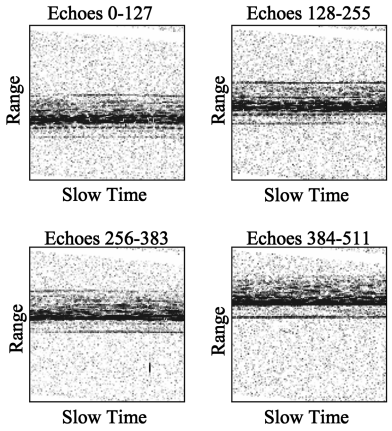

Fig. 3. Signals aligned by original global method.

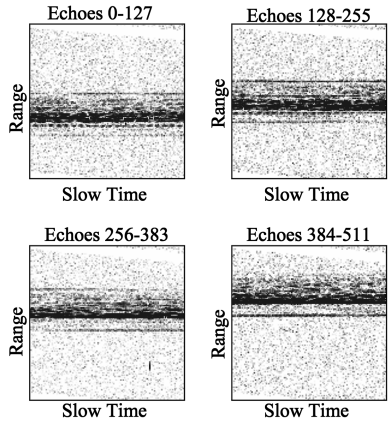

Fig. 4. Signals aligned by improved global method.

The field data of a Boeing-727 aircraft [17], provided by Professor B. D. Steinberg of the University of Pennsylvania, are used to evaluate our method. The aircraft was 2.7 km away from the radar and flew at a speed of 147 m/s. The radar transmitted short pulses at a wavelength of 3.123 cm and a width of 7 ns. The echoes were sampled at an interval of 5 ns; the pulse repetition frequency was 400 Hz; 512 echoes with 120 range bins each were recorded. The 512 echoes are divided into four equal segments, and each segment is processed individually.

Figs. 3–4 show the signals aligned in range by the original and the improved global methods, respectively. Phase adjustment and azimuth imaging have not been carried out yet here. As we see, the two methods have similar performance. They are robust against noise and target scintillation and avoid error accumulation.

Figs. 5–6 show the images based on the original and the improved global methods, respectively. Here,

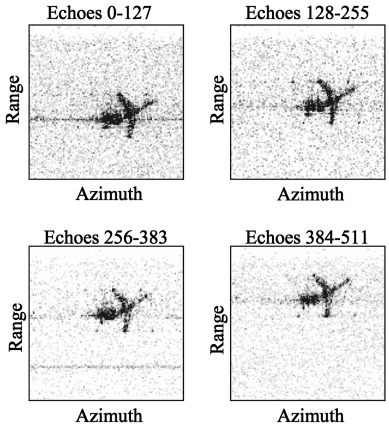

Fig. 5. Images based on original global method.

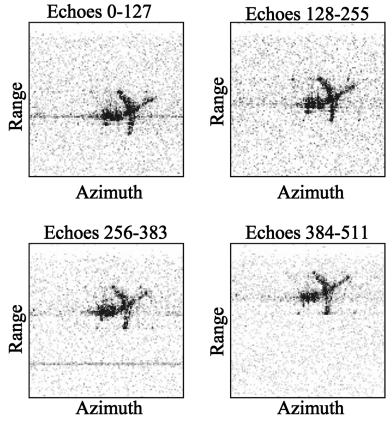

Fig. 6. Images based on improved global method.

the minimum-entropy method [15] is used for phase adjustment, and the Fourier transform is used for azimuth imaging. We can see that the two methods have similar performance. They both result in good focus quality.

Entropy can be used to measure the focus quality of an ISAR image [8, 14, 15]. Better focus results in smaller entropy. Thus, we can use entropy to evaluate the performance of the above two methods quantitatively. Table I gives the entropies of the images in Figs. 5 and 6. Here, entropy is calculated by

$$\varepsilon = -\sum_{l=0}^{M-1}\sum_{n=0}^{N-1} |g(l,n)|^2 \ln |g(l,n)|^2 \qquad (18)$$

where l is the index in azimuth, and $g(l,n)$ is the complex image [15]. As we can see, the entropy of the improved global method is equal to or less than that of the original global method for each set of echoes. This shows that the focus quality of the improved global method is the same as that of the original global method or even better.

Let us compare the computational efficiencies of the two methods. Table II gives the computation times of the two methods for four sets of echoes. The programs are written in Visual C++ 5.0 and run in Windows XP on a Dell Dimension 4600C PC (2.6 GHz Intel Pentium 4 processor and 512 MB memory). As we see, the improved global method has a higher computational efficiency than the original global method.

TABLE I
Entropies of Images in Figs. 5 and 6

	Original Global Method	Improved Global Method
Echoes 0–127	-6.53277×10^8	-6.60611×10^8
Echoes 128–255	-6.24596×10^8	-6.24596×10^8
Echoes 256–383	-8.01074×10^8	-8.01740×10^8
Echoes 384–511	-8.87984×10^8	-8.87984×10^8

TABLE II
Computation Times of Two Methods for Four Sets of Echoes

	Original Global Method	Improved Global Method
Echoes 0–127	1.297	0.187
Echoes 128–255	0.735	0.172
Echoes 256–383	1.094	0.172
Echoes 384–511	0.735	0.172

Note: unit: second.

IV. CONCLUSIONS

The improved global range alignment is effective and efficient in ISAR imaging. Like the original global method, it is robust against noise and target scintillation, avoids error accumulation, and removes the limitation of integer steps. Moreover, it is computationally more efficient than the original global method.

JUNFENG WANG
XINGZHAO LIU
Shanghai Jiaotong University
Shanghai, P.R. China 10085
E-mail: (junfengwang@sjtu.edu.cn)

REFERENCES

[1] Ausherman, D. A. Kozma, A., Walker, J. L., Jones, H. M., and Poggio, E. C.
Development in radar imaging.
IEEE Transactions on Aerospace and Electronic Systems, **AES-20**, 4 (July 1984), 363–400.

[2] Wehner, D. R.
High Resolution Radar (2nd ed.).
Norwood, MA: Artech House, 1994.

[3] Prickett, M. J., and Chen, C. C.
Principle of inverse synthetic aperture radar (ISAR) imaging.
In *IEEE EASCON Record*, 1980, 340–345.

[4] Pastina, D., Farina, A., Gunning, J., and Lombardo, P.
Two-dimensional super-resolution spectral analysis applied to SAR images.
IEE Proceedings of Radar, Sonar and Navigation, **145**, 5 (Oct. 1998), 281–290.

[5] Chen, V. C.
Joint time-frequency transform for radar range-Doppler imaging.
IEEE Transactions on Aerospace and Electronic Systems, **34**, 2 (Apr. 1998), 486–499.

[6] Chen, C. C., and Andrews, H. C.
Target-motion-induced radar imaging.
IEEE Transactions on Aerospace and Electronic Systems, **AES-16**, 1 (Jan. 1980), 2–14.

[7] Sauer, T., and Schroth, A.
Robust range alignment algorithm via Hough transform in an ISAR imaging system.
IEEE Transactions on Aerospace and Electronic Systems, **31**, 3 (July 1995), 1173–1177.

[8] Li, X., Liu, G., and Ni, J.
Autofocusing of ISAR images based on entropy minimization.
IEEE Transactions on Aerospace and Electronic Systems, **35**, 4 (Oct. 1999), 1240–1251.

[9] Wang, J., and Kasilingam, D.
Global range alignment for ISAR.
IEEE Transactions on Aerospace and Electronic Systems, **39**, 1 (Jan. 2003), 351–357.

[10] Eichel, P. H., Ghiglia, D. C., and Jakowatz, C. V.
Speckle processing method for synthetic aperture radar phase correction.
Optics Letters, **14**, 1 (Jan. 1989), 1–5.

[11] Wahl, D. E., Eichel, P. H,. Ghiglia, D. C., and Jakowatz, C. V.
Phase gradient autofocus—A robust tool for high resolution SAR phase correction.
IEEE Transactions on Aerospace and Electronic Systems, **30**, 3 (July 1994), 827–835.

[12] Barbarossa, S., and Farina, A.
A novel procedure for detecting and focusing moving objects with SAR based on the Wigner-Ville distribution.
In *IEEE International Radar Conference*, 1990, 44–50.

[13] Berizzi, F., and Cosini, G.
Autofocusing of inverse synthetic radar images using contrast optimization.
IEEE Transactions on Aerospace and Electronic Systems, **32**, 3 (July 1996), 1191–1197.

[14] Bocker, R. P., Henderson, T. B., Jones, S. A., and Frieden, B. R.
A new inverse synthetic aperture radar algorithm for translational motion compensation.
Proceedings of SPIE, vol. 1569, 1991, 298–310.

[15] Wang, J., Liu, X., and Zhou, Z.
Minimum-entropy phase adjustment for ISAR.
IEE Proceedings of Radar, Sonar and Navigation, **151**, 4 (Aug. 2004), 203–209.

[16] Wang, J., and Liu, X.
Improvement of ISAR global range alignment.
In *IEEE International Conference on Image Processing*, vol. 2, 2005, 217–220.

[17] Steinberg, B. D., and Subbaram, H. M.
Microwave Imaging Techniques.
New York: Wiley, 1991.

New Method of Chaotic Polyphase Sequences Design

A new polyphase sequences synthesis method based on chaotic maps is presented. The correlation properties of sequences designed using this method are analyzed and proved to be almost perfect. The phase alphabet size can be any positive non-zero even, and the alphabet elements can be chosen arbitrarily by users. Simulation results show the effectiveness of this polyphase sequences design method.

I. INTRODUCTION

To increase the average transmitted power while simultaneously maintaining adequate range resolution, pulse compression techniques, such as linear frequency modulation (LFM), binary phase modulation, polyphase modulation, and polytime codes [1] are often used in radar systems. In the modern battlefield, the application of electronic support measures (ESM), radar warning receivers (RWRs), and antiradiation missiles (ARMs) induce serious threats to radar. A lot of interception techniques have been introduced in the past 20 years [2–5]. Therefore, the performance of low probability of intercept (LPI) becomes an important requirement to modern radar. Polyphase signals and FM signals have a more complicated structure than binary phase signals. They are more difficult to detect and analyze by the enemy's ESM [6]. On the other hand, polyphase signals are easier to generate and process than chaotic FM signals because they have less phase states than FM signals. In fact, polyphase sequences [7–15] have been investigated a lot, but the number of orthogonal sequences is still limited. In multiradar systems, different radars must use sequences that are orthogonal to each other, so that they can work simultaneously. In monostatic radar systems, orthogonal polyphase sequences can be used to counter the coherent repeater jamming (CRJ) interferences [9]. The jammer receives radar signal and retransmits a replica to the radar receiver to interference it. If orthogonal radar signals are used in consecutive pulses, the jamming signal will not correlate with the current matched filter, and generate a near-zero output which has little effect on target

Manuscript received July 5, 2005; revised December 4, 2005 and June 4, 2006; released for publication March 15, 2007.

IEEE Log No. T-AES/43/3/908412.

Refereeing of this contribution was handled by M. Rangaswamy.